Earth System
Dynamics

Open Access

The sensitivity of the modeled energy budget and hydrological cycle to CO₂ and solar forcing

N. Schaller[1], **J. Cermak**[2], **M. Wild**[1], and **R. Knutti**[1]

[1]Institute for Atmospheric and Climate Science, ETH, Zurich, Switzerland
[2]Department of Geography, Ruhr-Universitaet Bochum, Bochum, Germany

Correspondence to: N. Schaller (nathalie.schaller@env.ethz.ch)

Abstract. The transient responses of the energy budget and the hydrological cycle to CO₂ and solar forcings of the same magnitude in a global climate model are quantified in this study. Idealized simulations are designed to test the assumption that the responses to forcings are linearly additive, i.e. whether the response to individual forcings can be added to estimate the responses to the combined forcing, and to understand the physical processes occurring as a response to a surface warming caused by CO₂ or solar forcing increases of the same magnitude. For the global climate model considered, the responses of most variables of the energy budget and hydrological cycle, including surface temperature, do not add linearly. A separation of the response into a forcing and a feedback term shows that for precipitation, this non-linearity arises from the feedback term, i.e. from the non-linearity of the temperature response and the changes in the water cycle resulting from it. Further, changes in the energy budget show that less energy is available at the surface for global annual mean latent heat flux, and hence global annual mean precipitation, in simulations of transient CO₂ concentration increase compared to simulations with an equivalent transient increase in the solar constant. On the other hand, lower tropospheric water vapor increase is similar between simulations with CO₂ and solar forcing increase of the same magnitude. The response in precipitation is therefore more muted compared to the response in water vapor in CO₂ forcing simulations, leading to a larger increase in residence time of water vapor in the atmosphere compared to solar forcing simulations. Finally, energy budget calculations show that poleward atmospheric energy transport increases more in solar forcing compared to equivalent CO₂ forcing simulations, which is in line with the identified strong increase in large-scale precipitation in solar forcing scenarios.

1 Introduction

Human activities primarily affect the climate system in two competing ways: greenhouse gases warm the atmosphere by partly absorbing longwave radiation, while aerosols have a predominantly cooling effect by scattering incoming shortwave radiation, although some of them also absorb radiation (Wild et al., 2008). Both forcing agents alter the energy budget of the Earth (Kiehl and Trenberth, 1997; Trenberth et al., 2009), which triggers responses through complex feedback mechanisms in order to reach a new equilibrium state. Among all these mechanisms, the ones modifying the processes leading to precipitation formation are of particular interest because human societies as well as ecosystems will likely be affected by changing precipitation patterns. Precipitation, and its energy equivalent, latent heat, are variables that belong to both the energy budget and hydrological cycle (e.g. Bosilovich et al., 2008; Liepert and Previdi, 2009; Alessandri et al., 2012), hence the need to analyze them jointly.

Recent studies have highlighted the dependency of precipitation changes on different emission scenarios, i.e. on the different forcing agents (Shiogama et al., 2010a; Lambert and Allen, 2009). It is widely accepted that the global mean precipitation change per unit temperature change is more sensitive to changes in aerosols or solar radiation than to changes in CO₂ concentrations (Allen and Ingram, 2002; Gillett et al., 2004; Andrews et al., 2009; Liepert and Previdi, 2009; Bala et al., 2010). This difference in precipitation response has been investigated from the perspective of the fast (weeks to months and caused by the forcing agent directly) and slow (years to centuries and caused by changes in surface temperature) responses (Lambert and Faull, 2007; Bala et al., 2008, 2010; Andrews et al., 2010; Cao et al., 2011). These studies found that the fast or forcing-dependent response of

precipitation is different for CO_2 and solar forcings, but that the slow or feedback-dependent response does not depend strongly on the nature of the forcing agent. Increasing CO_2 concentrations lead to small but rapid increases in tropospheric temperatures, while surface temperature remains unchanged initially. Atmospheric stability is increased, reducing convection and therefore precipitation in the first days to months (Andrews et al., 2010). In addition, Andrews et al. (2011) and Cao et al. (2012) showed that on timescales of a few days and over land, increasing CO_2 concentrations lead to a reduction in plant transpiration, which also contributes to precipitation reduction. While increasing solar radiation leads to an increased absorption of shortwave radiation in the atmosphere, also inducing a weak reduction in precipitation on short timescales, this direct effect of the forcing agents is almost negligible compared to that of CO_2 (O'Gorman et al., 2012).

Another important aspect in the discussion on how the climate system responds to forcings is the assumption of linear additivity, i.e. whether the responses to individual forcings can be added to estimate the response to the combined forcing. While Meehl et al. (2004) found this assumption to be valid for the global mean response to the twentieth-century forcings, Mitchell (2003) showed that some significant errors can be introduced by this assumption. Meehl et al. (2003) further showed that the model's temperature response to solar forcing is amplified when it is combined with anthropogenic forcings, which they interpreted as a non-linear response of the climate system to solar forcing. Results presented in Jonko et al. (2012) also suggest that global mean surface temperature difference neither exactly doubles from $2 \times CO_2$ to $4 \times CO_2$ nor from $4 \times CO_2$ to $8 \times CO_2$. Testing the linear additivity of the global mean temperature change is particularly relevant for impact studies based on pattern scaling. This technique relies on the fact that the scaled pattern of change of surface variables in any scenario is approximately constant over time (Santer and Wigley, 1990). The resulting main advantage is that Global or Regional Climate Models (GCMS or RCMs) do not need to actually simulate all scenarios since the information about the pattern of change is approximately the same for all scenarios (Giorgi, 2008). Pattern scaling has been widely used for temperature and precipitation (e.g. Mitchell and Hulme, 1999; Meehl et al., 2007; Watterson, 2008). Recently Shiogama et al. (2010a) showed that the technique is less reliable for precipitation patterns, which are more sensitive to the nature of the forcing agent, and Shiogama et al. (2010b) identified a potential overestimation of the changes in precipitation with pattern scaling. Besides the assumption that the pattern of change remains the same under low and high forcings and under forcings caused by different agents, another assumption needs to be made about the scaling factor. Global mean temperature change is usually used as the scaling factor and is estimated with energy balance models (Ruosteenoja et al., 2007). However, Good et al. (2012) identified with a simple climate model

substantial deviations from the linear scaling with global mean temperature for precipitation response in some regions. Using energy balance models is limited because their global mean temperature response does not depend on the nature of the forcing but only on their total radiative perturbation, unless efficacies for individual forcings are individually prescribed. In the way forcing agents are implemented in these models, the assumption that the temperature response to forcings is linear is made, except if the feedback parameter is parametrized as a function of the forcing.

Many previous studies quantified the climate responses in simulations where the forcing is increased instantaneously (e.g. Bala et al., 2010). While much can be learned from those, there is also currently a need to understand transient climate change since this is more relevant for adaptation strategies. The two goals of this study are therefore to test the assumption of linear additivity for a broad range of variables using transient solar and CO_2 forcing increase simulations in a GCM and to quantify the transient response of the energy budget and the hydrological cycle to different forcing agents, globally and zonally. A description of the climate model experiments is provided in Sect. 2. Section 3 summarizes the results and discusses the two key aspects considered, the assumption of the linear additivity of the responses to different forcing agents or forcing magnitudes, and the differences in the energy budget and hydrological cycle responses depending on the forcing agent. The conclusions are presented in Sect. 4.

2 Climate model simulations and methods

A set of idealized transient simulations is performed with the NCAR Community Climate System Model version 3.5 (CCSM3.5) (Collins et al., 2006; Gent et al., 2010). The finite volume dynamical core of this fully coupled ocean and atmosphere model has a spatial resolution of 1.9° in latitude and 2.5° in longitude, with 26 levels in the vertical. The physics of cloud and precipitation processes include a separate prognostic treatment of liquid and ice condensate, advection, detrainment, and sedimentation of cloud condensate and separate treatments of frozen and liquid precipitation (Boville et al., 2006; Collins et al., 2006). The inclusion of the effects of deep convection in the momentum equation lead to improvements in the representation of ENSO, the Asian monsoon and the double-ITCZ problem in the eastern Pacific Ocean (Gent et al., 2010).

First, a 600 yr present-day control simulation is run with the CCSM3.5 model and equilibrium is reached after around 150 yr. The simulations with CO_2 and solar forcings are ensemble members that branch out at years 400, 430, 450, 470 and 500 of the control simulation to sample different initial conditions. Each case (scenario hereafter) therefore consists of five initial condition ensemble members to quantify the model internal variability. The first scenario is

a 1 % yr^{-1} transient increase of CO_2 up to doubled values (from 355 ppm up to 710 ppm and labeled "C2x" hereafter). The next scenario is a 2 % yr^{-1} increase in CO_2 (from 355 to 1420 ppm and labeled "C4x" hereafter). Then, to investigate the response of the energy budget and hydrological cycle to changes in solar radiation, the solar constant is transiently increased relative to the control value to reach a radiative forcing that corresponds theoretically to a doubling or quadrupling of CO_2. According to the best estimate provided by Myhre et al. (1998), the radiative forcing of a doubling in CO_2 concentrations would be about 3.7 W m^{-2}. Correspondingly, in the solar forcing simulations the solar constant is increased by the best estimate radiative forcings ΔF corresponding to each CO_2 scenario (i.e. 3.7 W m^{-2} or 7.4 W m^{-2}) multiplied by 4 (to account of the geometry of the Earth) and divided by 0.7 (the planetary albedo being approximately 0.3). The two solar scenarios are labeled "S37" and "S74". Finally, a scenario with a 1 % yr^{-1} increase in CO_2 and an increase in solar forcing that reaches a 3.7 W m^{-2} radiative forcing at the end of the simulation is run (labeled "S37C2x"). In addition, a 25 yr simulation starting in year 400 for each scenario is performed with instantaneous increase of the forcing agents ($2 \times CO_2$, $4 \times CO_2$, 3.7 W m^{-2}, 7.4 W m^{-2} and $2 \times CO_2$ combined with 3.7 W m^{-2}) to infer the adjusted forcing. The adjusted forcing is different form the radiative forcing in that it includes the rapid adjustments occurring within a few days in the troposphere and land surface (Forster et al., 2013). The method by Gregory et al. (2004) is used to estimate the adjusted forcing as the intercept in a linear regression of changes in net radiation at top of atmosphere (TOA) against the changes in surface temperature.

The end of the transient phase of all five scenarios is reached during year 69 relative to the branching point of the scenarios, and for the rest of the study, we consider annual mean anomalies of the years 71 to 100 compared to the average over 100 yr in the control simulation. All fluxes are defined as positive downward and consequently, positive anomalies represent a gain of energy for the surface, and negative ones, a loss. Figure 1a shows the time series of the global annual mean surface temperature anomaly for the five scenarios.

As mentioned before, the scenarios are designed to test the assumption of linear additivity in the response to solar and CO_2 forcings. If the assumption is valid, scaling the global mean response at the end of the simulation in any variable in the C2x scenario by the adjusted forcing in C2x should be equal to the scaled responses in the C4x scenario. Similarly, scaling the global mean responses in the S37 scenario by its adjusted forcing should give similar results as the scaled responses in the S74 scenario. Finally, adding the responses of the C2x and S37 scenario and scaling them by the sum of the adjusted forcing in S37 and C2x should be equal to the scaled responses in the S37C2x scenario. A two-sample Kolmogorov–Smirnov test with significance level 0.05 is
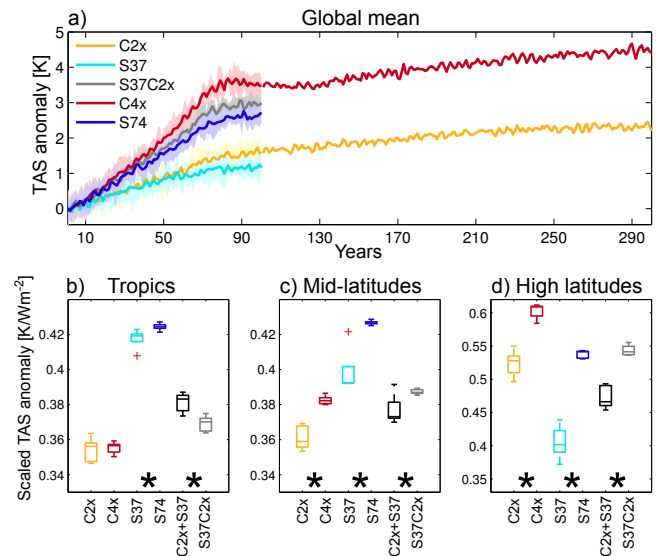

Fig. 1. (a) Time series of the global annual mean anomaly of surface air temperature (TAS) [K] for all five scenarios. Averages over five initial condition ensemble members for the 100 yr simulations and over 3 members for the 300 yr simulations are shown. Shading extends from the lowest to highest value obtained by any of the five ensemble members. Regional surface air temperature anomalies scaled by the adjusted forcing [K Wm^{-2}] in the scenarios are shown for **(b)** the tropics, **(c)** the mid-latitudes and **(d)** the high latitudes (see text for definition of the sub-regions). Asterisks are displayed whenever the pairs of scenarios (C2x and C4x, S37 and S74, S37C2x and C2x + S37) are significantly different from each other (two-sample Kolmogorov–Smirnov test, significance level 0.05) and therefore indicate when the linear additivity assumption is not valid. Red crosses are outliers.

used to assess whether the distributions of the five ensemble members of two scenarios (the scaled C2x and scaled C4x for example) are statistically significantly different.

3 Results and discussion

3.1 Linear additivity of the responses

As discussed in the Introduction, the assumption that the responses to individual forcings are linearly additive is widely made in climate science, in particular in the fields of detection and attribution (Barnett et al., 2005) or pattern scaling (Mitchell, 2003). Pattern scaling approaches are based on the fact that the response pattern in one scenario is very similar to the pattern in another scenario. For the idealized simulations performed in this study, all response patterns of variables from the energy budget and hydrological cycle are highly correlated. As an example, the response pattern of total precipitation averaged over the last 30 yr of each scenario has a correlation coefficient, ρ, of 0.93 between C2x and C4x and of $\rho = 0.91$ between S37 and S74. Even between
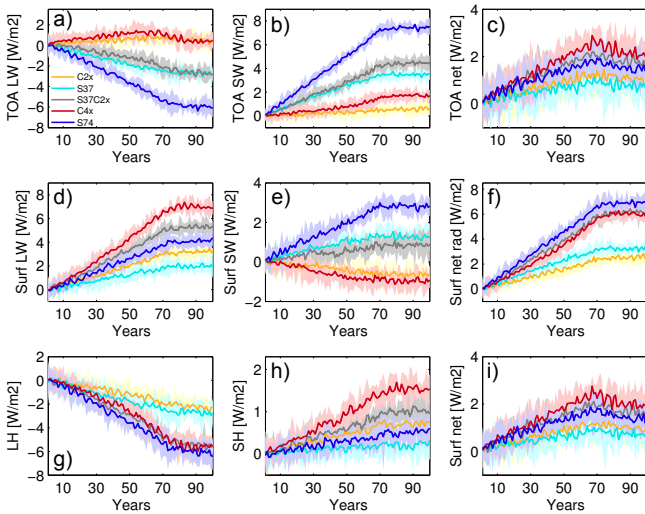
Fig. 2. Global annual mean anomalies of selected components of the energy budget. Averages over five ensemble members are shown and shading extends from the lowest to the largest value obtained by any of the five ensemble members. **(a)** top of atmosphere longwave flux, **(b)** top of atmosphere net shortwave flux, **(c)** top of atmosphere net radiative flux, **(d)** surface net longwave flux, **(e)** surface net shortwave flux, **(f)** surface net radiative flux, **(g)** latent heat flux, **(h)** sensible heat flux and **(i)** surface net radiative and turbulent flux. All fluxes are in W m^{-2} and are defined as positive downward.

the different forcing agents, correlation coefficients are high ($\rho = 0.94$ between C2x and S37 and $\rho = 0.92$ between C4x and S74). Pattern scaling techniques further make the assumption that the responses to different forcing agents or to forcing agents of different intensity add linearly. Here we test the linear additivity assumption for changes in global mean temperature and changes in variables of the energy budget and hydrological cycle in a GCM. The objective of this section is not to make any judgment on the validity of the mentioned techniques. Depending on the purpose, it can be then be decided whether the errors introduced by the assumption of linear additivity are negligible or not.

First, we use the instantaneous forcing increase simulations described in the previous section and the method proposed in Gregory et al. (2004) to estimate the adjusted forcing in each scenario. There are, however, other ways to estimate the radiative forcing, as described in Hansen et al. (2002) or Shine et al. (2003). The adjusted forcing is 3.77 W m^{-2} for the C2x scenario, 8.15 W m^{-2} for C4x, 2.81 W m^{-2} for S37, 5.61 W m^{-2} for S74 and 6.84 W m^{-2} for S37C2x. The adjusted forcing in the C2x scenario agrees well with the theoretical value from Myhre et al. (1998). However, the adjusted forcing in the C4x scenario is larger than expected, and the ratio of adjusted forcings between C4x and C2x is 2.16. For the solar scenarios, the ratio of adjusted forcings is indeed 2 but the adjusted forcings are smaller than expected. Hansen et al. (2005) and Schmidt et al. (2012)

showed that the efficacy of solar forcing is smaller than that of CO$_2$ forcing. The net shortwave flux is indeed as prescribed, 3.7 W m^{-2} and 7.4 W m^{-2} (see Fig. 2b), however the increase in net longwave flux, due to the black-body response of the warmer surface (see Fig. 2a), compensates the incoming solar energy, and the net energy flux at TOA is small. Changes in energy fluxes in the scenarios will be further discussed in the next section. The fact that the adjusted forcings do not add linearly in the CO$_2$ scenarios and that the adjusted forcings in solar simulations are lower than expected from Myhre et al. (1998) are important since such results cannot be obtained from simple energy balance models. In these models, all forcing agents are added into a total radiative forcing value, and by construction, there is no forcing-dependency of the temperature response (except if it is explicitly parametrized).

The linear additivity assumption is tested for variables of the energy budget and hydrological cycle and results are presented in Table 1. The response in a given variable in a low scenario scaled by the adjusted forcing in this scenario is compared with the response in the scaled high forcing scenario. A two-sample Kolmogorov–Smirnov test is used to assess if the five ensemble members of the compared scenarios are significantly different. In Table 1, the differences (response of the scaled high forcing scenarios minus scaled response of the low forcing scenarios) are shown as percentages of the reference value, i.e. the scaled responses to the low forcing scenarios. Positive and negative values therefore mean that for a given variable, the high forcing scenario responses are significantly larger and smaller, respectively, than expected from the linear additivity assumption. No values are shown for variables where the linear additivity assumption is valid, i.e. differences are not significantly different. Since the responses are scaled by the adjusted radiative forcing, the values shown represent non-linearities arising from long-term feedbacks. Overall, the results shown in Table 1 indicate that the linear additivity assumption is not valid for most variables and in general, the responses to high forcings are larger than expected. This is in line with, e.g., Good et al. (2012), who showed that with increasing CO$_2$ levels, the longwave emission level raises, implying a colder emission temperature and therefore a reduced Planck function response. Differences on the order of 10 % might be considered acceptable for some applications, given that model or observational uncertainties are potentially much larger. As an example, Mitchell (2003) concludes that pattern scaling is generally accurate with significant errors not exceeding 2.8 % of the global mean temperature change and 11 % of the global mean precipitation change. Results obtained with the CCSM3.5 model show much larger differences. One could argue that these errors are avoidable as computational capacity is becoming less of a limiting factor for any given model, but on the other hand models are getting more expensive, such that the wall-clock time spent for a single simulation has remained remarkably constant over the past decades.

Table 1. Results from the linear additivity test on chosen variables of the energy budget and hydrological cycle scaled by the adjusted forcing in the scenario. Positive values indicate that the high forcing scenario has a larger response than expected doubling/addition of the low forcing scenarios. Only statistically significant differences are shown, the linear additivity assumption is valid where no value is given.

	CO_2 scaled C4x vs. scaled C2x	solar scaled S74 vs. scaled S37	CO_2 + solar scaled S37C2x vs. scaled C2x + S37
TOA SW net ($W\,m^{-2}$)	41.5 %	6.6 %	5 %
TOA LW net ($W\,m^{-2}$)	−54.8 %	9.2 %	16.1 %
TOA net ($W\,m^{-2}$)	−6.6 %	–	−7.4 %
Total cloud cover (%)	−5.3 %	11.7 %	–
High cloud cover (%)	−37.2 %	–	−91.6 %
Mid-level cloud cover (%)	–	–	–
Low cloud cover (%)	6.7 %	11.6 %	9.5 %
Surface SW net ($W\,m^{-2}$)	−32.4 %	11.6 %	33 %
Surface LW net ($W\,m^{-2}$)	1.6 %	3.8 %	−1.6 %
Surface radiative net ($W\,m^{-2}$)	10.4 %	6.8 %	2 %
Sensible heat flux ($W\,m^{-2}$)	–	16.3 %	3.8 %
Latent heat flux ($W\,m^{-2}$)	15.4 %	10.8 %	6.3 %
Surface net ($W\,m^{-2}$)	−7.6 %	−4.1 %	−8.5 %
Precipitable water (mm)	9.7 %	10.6 %	5.9 %
Total precipitation ($mm\,day^{-1}$)	15.5 %	10.8 %	6.4 %
Large-scale precipitation ($mm\,day^{-1}$)	20.4 %	–	–
Convective precipitation ($mm\,day^{-1}$)	13.4 %	18.9 %	9.7 %
Surface temperature (K)	7.6 %	12 %	4.8 %

However, other sources of errors are less easy to get rid of, for example structural or observational uncertainties.

As mentioned above, the system is obviously not in equilibrium 30 yr after the transient forcing increase and this is one reason for the non-validity of the linear additivity assumption. Even though for global mean temperature and in simple models, the ratio of warming per unit forcing is roughly constant even for the transient case (Gregory and Forster, 2008; Knutti et al., 2008), that is unlikely to hold for other variables and local changes. Long model simulations show that it takes hundreds of years to reach equilibrium (Gregory et al., 2004; Stouffer, 2004). Even after 300 yr, scenarios with CO_2 forcing (see Fig. 1a) show that the system is not in equilibrium, as surface temperature continues to rise. However, there is currently a need for assessments of transient climate change since this is more relevant for the real world, the climate system never reaching a true equilibrium. In the recently published Representative Concentration Pathways (RCP) scenarios, stabilization of the forcings do not occur before 2100 and some pathways are even bell-shaped, with stabilization occurring after 300 yr (Moss et al., 2010). The fact that the response of most variables does not scale linearly with the forcing in transient climate changes has important implications for the scaling of climate change patterns based on simple energy balance models.

3.2 Temperature response and forcing-feedback decomposition

For the rest of the study, the responses are scaled by their respective adjusted forcings only in figures concerning the linear additivity assumption, i.e. Figs. 1b, c, d and 5. In the other cases, the raw responses will be considered, for several reasons. First, scaling the responses would make the assumption that each variable at each grid point scales linearly with the adjusted forcing. While scaling the responses of global or continental temperature might be justified (Meehl et al., 2004), other quantities such as the zonal mean profile of specific humidity or residence time of water vapor in the atmosphere cannot necessarily be scaled with the adjusted forcing. Further, the differences in the raw responses between CO_2 and solar scenarios that will be discussed below are large and scaling the responses would not change the conclusions and/or make those differences even larger.

The larger temperature changes at the surface in the CO_2 compared to solar scenarios seen in Fig. 1a are caused by the larger adjusted forcing values mentioned above. The scaled global mean surface temperature anomalies are almost the same for the CO_2 and solar cases, although slightly larger in the solar cases, indicating that solar forcing is more efficient at warming the surface. As seen in Fig. 1a for the C4x scenario, the temperature increase appears to be strong during the first 70 yr but after CO_2 concentrations remain constant, a decrease occurs, followed by a slow increase. This

"overshoot" comes from the northern high latitudes (see region definitions below), the temperature increase is monotonic in the other sub-regions (not shown). An explanation for this behavior might be that when the Meridional Overturning Circulation (MOC) is reduced (as occurs in warming scenarios) the ocean transiently takes up a lot of energy, which is compensated by a temporary decrease in atmospheric temperature (Knutti and Stocker, 2000). It is however difficult to judge whether this mechanism is a robust response of the climate system or just a feature of the CCSM3.5 model.

Motivated by the fact that precipitation in CCSM3.5 is expected to increase in high latitudes and near the equator but decrease in mid-latitudes (see Schaller et al., 2011, Fig. 3), anomalies are also computed for three sub-regions: the tropics (15° S–15° N), the sub-tropics and mid-latitudes (50° S–15° S and 15° N–50° N), which will be referred to as mid-latitudes for simplicity in the rest of the text, and the high latitudes (90° S–50° S and 50° N–90° N). The surface temperature anomalies of the last 30 yr of each simulation scaled by their respective adjusted forcings are shown in Fig. 1b–d for the three sub-regions. According to the Kolmogorov–Smirnov test, all but one pair of scenarios are significantly different from each other, indicating that the non-validity of the linear additivity assumption does not depend on the region considered in solar scenarios but that it arises from higher latitudes in CO_2 scenarios. Figure 1b-d further shows that the scaled annual mean temperature responses to CO_2 and solar forcing in different regions are significantly different, although the idea underlying the radiative forcing concept would suggest that they are similar. The scaled surface temperature response to solar forcing is larger at low latitudes while it is larger at high latitudes in the CO_2 scenarios. This results from the fact that solar forcing acts primarily at low latitudes and, although also present in solar scenarios, polar amplification is stronger in CO_2 scenarios.

As a further step to investigate the non-linearity of the responses, the method described by Andrews (2009) is used to separate the total response into a part caused by the forcing directly and a part resulting from the change in surface temperature, i.e. the feedback-dependent part. We repeat the same analysis as in Andrews (2009) for the five ensemble members of all CO_2 and solar scenarios and for the energy budget fluxes as well as precipitation. The anomaly N_i in a given flux i is given by

$$N_i = F_i - \alpha_i \Delta T, \tag{1}$$

where F_i is the part of this anomaly caused by the forcing directly, α_i is the feedback parameter for the given energy flux i, and ΔT is the change in surface temperature. By regressing the annual mean values from year 71 to 100 of N_i against the annual mean values of ΔT, one can determine the feedback parameters α_i for each of the five ensemble members separately in the five different scenarios. Once α_i is determined, the forcing F_i and feedback parts $\alpha_i \Delta T$ can be calculated for
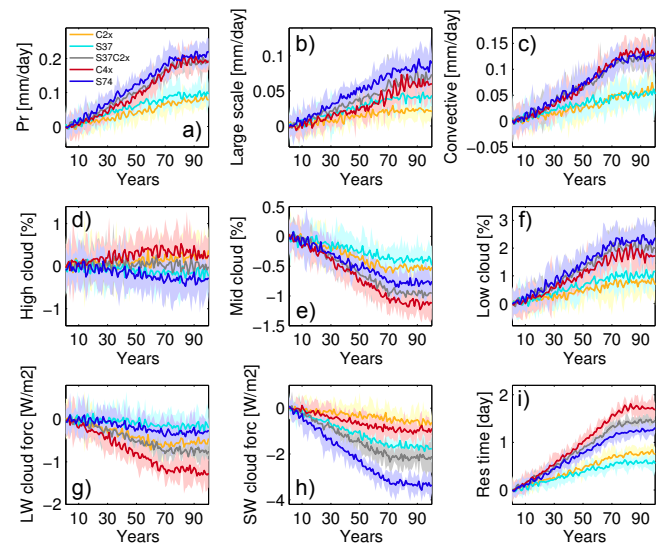

Fig. 3. Global annual mean anomalies of selected components of the hydrological cycle. Averages over five ensemble members are shown and shading extends from the lowest to the largest value obtained by any of the five ensemble members. (a) total precipitation [mm day^{-1}], (b) large-scale precipitation [mm day^{-1}], (c) convective precipitation [mm day^{-1}], (d) high cloud fraction [%], (e) mid-level cloud fraction [%], (f) low cloud fraction [%], (g) longwave cloud radiative forcing [W m^{-2}], (h) shortwave cloud radiative forcing [W m^{-2}] and (i) residence time [day].

each of the five ensemble members, again separately, in the five scenarios. Andrews (2009) assumes that the feedback parameters are forcing-independent. We find this assumption to be valid in our CO_2 and solar forcing scenarios (not shown). For most variables however, the feedback parameters appear not to be well constrained in CCSM3.5. Reasons might be that the inter-annual variability is large or that the climate change signal is weak for those variables. The feedback parameter for precipitation however is well constrained and repeating the linear additivity test shows that the non-linearity arises from the feedback part in both CO_2 and solar forcing scenarios. The forcing part adds linearly but the feedback part is larger by 36 % in C4x compared to C2x and by 20 % in S74 compared to S37. This is expected since temperature also behaves non-linearly as shown previously. Further, the regression method applied to CCSM3.5 confirms results from previous studies showing that the forcing contribution is negative in CO_2 scenarios but close to zero in the solar case (Bala et al., 2010; Andrews and Forster, 2010; Cao et al., 2011). The feedback part is positive for CO_2 and solar forcings but is larger in the CO_2 case since it follows the larger temperature increase in these unscaled scenarios. For the rest of the study the focus will be on differences in the processes, and therefore the comparison between CO_2 and solar scenarios of the same intensity.

3.3 Dependency on the forcing agent

3.3.1 Changes in the energy budget

The net shortwave (SW) flux change at TOA in the solar scenarios roughly corresponds to the imposed solar forcings as shown in Fig. 2b. This is not necessarily the case in all models, but in CCSM3.5 the SW clear-sky flux change is very large (around $11\,\mathrm{W\,m^{-2}}$ in S74) and is offset by a relatively large increase in SW cloud radiative forcing (SWCRF) of more than $3\,\mathrm{W\,m^{-2}}$ (see Fig. 3h). The net SW flux change in the CO_2 scenarios is much smaller than the SW clear-sky flux change and cloud radiative forcing. In the solar scenarios, the longwave (LW) fluxes become more negative, indicating that as a consequence of the heating of the surface (and the atmosphere to a lesser extent), the Earth emits more LW radiation to space (see Fig. 2a). In the CO_2 scenarios, the surface and atmosphere also warm during the simulation but the increasing CO_2 concentrations trap the upward LW radiation, hence a positive anomaly at TOA. For TOA LW, the differences between high and low forcing scenarios are much larger for solar than for CO_2 scenarios, where the values are almost the same. This is due to the strongly negative LW cloud radiative forcing in C4x (see Fig. 3g), which might be due to the fast cloud adjustments to CO_2 as shown by Gregory and Webb (2008).

The response of the system at TOA to solar forcing is large in both the SW and LW compared to the relatively small responses at TOA for CO_2 forcing, although one might expect that solar forcing would act mostly in the SW range and CO_2 in the LW range (Meehl et al., 2003; Bala et al., 2010). Still, the net TOA flux anomalies are in the same range for both forcings and would be almost equal if they were scaled by their respective adjusted forcing values (see Fig. 2c). Looking at the net energy flux changes at the surface (turbulent and radiative) in Fig. 2i, the picture is very similar, indicating that the atmosphere only takes up a small part of the increased energy in the system. This is consistent with observations indicating that most of the excess energy is taken up by the oceans (Levitus et al., 2001).

Considering the SW and LW fluxes at the surface again highlights the different processes occurring in the CO_2 and solar scenarios. While less SW radiation is absorbed by the surface in the CO_2 scenarios compared to the control simulation, the opposite is true in the solar scenarios (see Fig. 2e). Besides the obvious fact that there is less net SW radiation at TOA in CO_2 compared to solar scenarios, this outcome can be further explained by an increase in low clouds in CO_2 scenarios (see Fig. 3f) rather than by changes in surface albedo. The time series of the surface net LW flux anomalies reflect surface warming and show the large increase in back radiation in the CO_2 scenarios (see Fig. 2d). In those scenarios, changes in LW back radiation are caused by increases in CO_2 (although Allan (2006) showed that this effect is small in the tropics), water vapor and low clouds, while in

the solar scenarios, only the increasing greenhouse effect of water vapor and low clouds is seen. In addition, changes in surface temperature are larger in CO_2 scenarios, which in itself causes a larger increase in water vapor and consequently larger back radiation.

Changes in global annual mean precipitation can be understood either from an atmospheric (Mitchell et al., 1987; Allen and Ingram, 2002; Liepert and Previdi, 2009; Alessandri et al., 2012) or a surface energy budget perspective (Boer, 1993; Wild et al., 2008; Andrews et al., 2009). Both interpretations have been shown to be valid and from a surface energy budget point of view, changes in the global hydrological cycle are primarily driven by changes in the energy available at the surface for the turbulent energy fluxes. The increase in net surface radiative flux, i.e. the sum of the changes in net surface LW ΔLW_{surf} and in net surface SW ΔSW_{surf} (left hand side of Eq. 2 and Fig. 2f), indicates that there is potentially more energy available at the surface for evaporation in the solar than in the corresponding CO_2 scenarios, mostly due to the negative surface SW anomaly in the CO_2 scenarios. In this case, a scaling of the variables would make the differences between CO_2 and solar scenarios even larger.

$$\Delta LW_{surf} + \Delta SW_{surf} = \Delta NET_{surf} - (\Delta LH + \Delta SH) \quad (2)$$

The change in net radiative flux at the surface is partitioned into changes in latent and sensible heat flux (ΔLH and ΔSH respectively) and some of the excess energy will be taken up by the ocean or land surface (ΔNET_{surf}). Two aspects control the partitioning of the available energy: the surface and the atmosphere. On one hand, over oceans and wet land, changes in latent heat flux dominate but over a dry surface, no water can be evaporated and therefore the available energy goes into sensible heat (Sutton et al., 2007). On the other hand, if more energy is available for evaporation, this increased evaporation rate can only be sustained if the evaporated water vapor is removed from the boundary layer by convective processes. In all scenarios, the latent heat flux increases (see Fig. 2g) and the sensible heat flux decreases, with a strong dependence on the forcing agent (see Fig. 2h). SH decreases due to a decrease in the air-sea temperature difference at the surface, caused by an increased opacity in the LW of the atmosphere associated with the increase in specific humidity (see Fig. 4b and d) (Stephens and Ellis, 2008; O'Gorman et al., 2012). The SH decrease is less pronounced in solar scenarios due to the fact that solar forcing primarily acts at warming the surface, while CO_2 forcing induces a warming of the whole troposphere. Those changes are however dominated by the ocean response, where water availability is unlimited: over land, the increase in LH is weaker since soil moisture is not available in all regions or due to boundary layer processes, and SH slightly increases (around $1\,\mathrm{W\,m^{-2}}$).
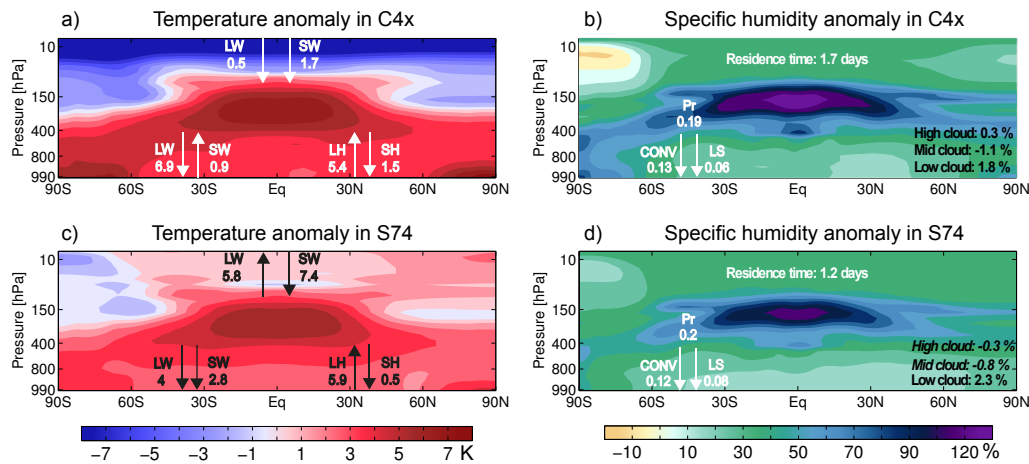
Fig. 4. Profiles of (**a**) the annual mean anomaly in temperature [K] and (**b**) the change in specific humidity [%] in the C4x scenario. (**c, d**) as in (**a, b**) but for the S74 scenario. The mean anomalies over the five ensemble members averaged over the years 71 to 100 of the corresponding scenario are indicated on the profiles. The energy fluxes are defined as positive in the direction of the corresponding arrow. The units of the energy flux anomalies in (**a**) and (**c**) are in $W\,m^{-2}$ and the units of the precipitation variables in (**b**) and (**d**) are in $mm\,day^{-1}$. Anomalies written in italics indicate that the linear additivity assumption is valid for this variable.

3.3.2 Changes in the hydrological cycle

Understanding how clouds will change in the future remains a major challenge since climate models have difficulties in simulating low clouds in particular (Stephens, 2005; Zhang et al., 2005). Total cloud cover increases in all five scenarios with no strong dependency on the forcing agent (not shown), but most CMIP3 and CMIP5 models actually show a decrease in total cloud cover (Bender, 2011; Andrews et al., 2012). Gregory and Webb (2008) as well as Andrews and Forster (2008) showed that fast cloud adjustments caused by an increase in CO_2 forcing are responsible for most of the spread among models. After removing these fast adjustments, cloud feedbacks appear more consistent in the different models. Low cloud cover increases more in solar scenarios as shown in Fig. 3f. These clouds likely have a cooling effect because they reflect SW radiation, which would act as a negative feedback to the climate system. The changes in high-level cloud cover shown in Fig. 3d are very small and they should be interpreted carefully. However, Zelinka and Hartmann (2010) showed that small changes in cloud top emission temperature are more critical for the LW cloud feedback than changes in high cloud cover. Overall, increasing high cloud cover could lead to more warming because high clouds may trap upward LW radiation, which would imply a positive feedback in CO_2 scenarios and a negative feedback in solar scenarios due to the slight increase and decrease in high cloud cover, respectively, in these scenarios.

Vertical profiles of temperature anomalies in C4x and S74 are shown in Fig. 4a and c respectively. The warming of the troposphere and cooling of the stratosphere is characteristic for CO_2-induced climate change, while the stratosphere is warming overall in solar scenarios. Given the

Clausius–Clapeyron relationship, atmospheric water vapor change will closely follow temperature change, at a rate of around $7\,\%\,K^{-1}$ for temperatures typically found at the surface, but by a rate of around $15\,\%\,K^{-1}$ at temperatures encountered in the upper troposphere. In the lower troposphere, the temperature increase is stronger in the unscaled CO_2 scenarios and consequently, specific humidity increases more relative to solar scenarios, as shown in Fig. 4b and d. On the other hand, latent heat flux increases more in solar scenarios, hence a larger precipitation increase compared to CO_2 scenarios (see Fig. 3a). Mitchell et al. (1987) showed that changes in precipitation due to warming occur at a smaller rate than changes in water vapor because the former are limited by the energy balance of the atmosphere. Even though both specific humidity and precipitation increase with warming, there is a difference between their respective increase rates, which must be compensated by a weakening of the atmospheric circulation (Held and Soden, 2006). In global climate model projections, Held and Soden (2006) found that the change in convective mass flux is expected to decrease as a consequence of the fact that precipitation increases only by about $2\,\%\,K^{-1}$ while water vapor increases by $7\,\%\,K^{-1}$. Here, the precipitation response in CO_2 scenarios is more muted compared to the response in water vapor than in solar scenarios. A weakening of the atmospheric circulation is equivalent to an increase in residence time of water vapor in the atmosphere, i.e. the ratio between total precipitable water and global precipitation rate, as shown by Douville et al. (2002) and Bosilovich et al. (2005). The residence time in the control simulation is around nine days and it increases in all scenarios by as much as two days (see Fig. 3i). However, the residence time of water in the atmosphere is larger in CO_2 scenarios compared to solar scenarios of the same
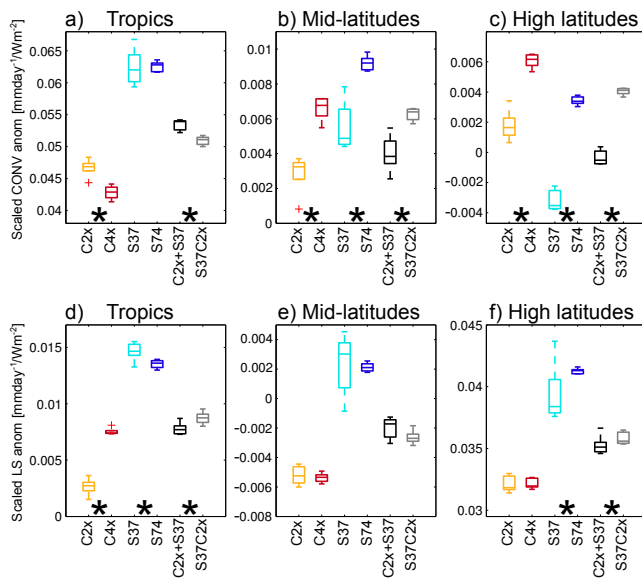
Fig. 5. Annual mean anomalies for convective (CONV) and large-scale (LS) precipitation in the tropics (**a** and **d** respectively), the mid-latitudes (**b** and **e** respectively) and the high latitudes (**c** and **f** respectively). Anomalies in all scenarios are scaled with their respective adjusted forcing and units are therefore [mm day^{-1} Wm^{-2}]. See text for definition of the regions and values of the adjusted forcing in each scenario. Asterisks are displayed whenever the pairs of scenarios (C2x and C4x, S37 and S74, S37C2x and C2x + S37) are significantly different (two-sample Kolmogorov–Smirnov test, significance level 0.05) and therefore indicate when the linear additivity assumption is not valid. Red crosses are outliers.

Fig. 6. Annual mean meridional surface air temperature gradient calculated as the difference between 15° S–15° N and 90° N–50° N or 50° S–90° S for (**a**) the Northern (NH) or (**b**) the Southern Hemisphere (SH) for all five scenarios. Averages over the five ensemble members are shown.

intensity, implying a weaker atmospheric circulation in the CO_2 scenarios. Since residence time is defined as the ratio of two variables, scaling the responses would lead to the same result.

To obtain additional information on the processes responsible for changes in precipitation, changes in large-scale and convective precipitation are considered separately. The unscaled time series of global mean anomalies in large-scale and convective precipitation are shown in Fig. 3b–c and the scaled regional anomalies for large-scale and convective precipitation are shown in Fig. 5. The linear additivity assumption is also tested in the three sub-regions in a similar way as in Fig. 1b–d. For convective precipitation, the linear additivity assumption is almost never valid (see Fig. 5a–c) and in the high latitudes, the direction of change is even inverted between S37 and S74. For large-scale precipitation, the assumption of linear additivity is valid in mid-latitudes for all scenarios but also in high latitudes for the CO_2 cases (see Fig. 5d–f). The invalidity of the linear-additivity assumption therefore cannot easily be attributed to specific regions. However, large-scale precipitation processes seem to be better represented by the assumption than convective precipitation.
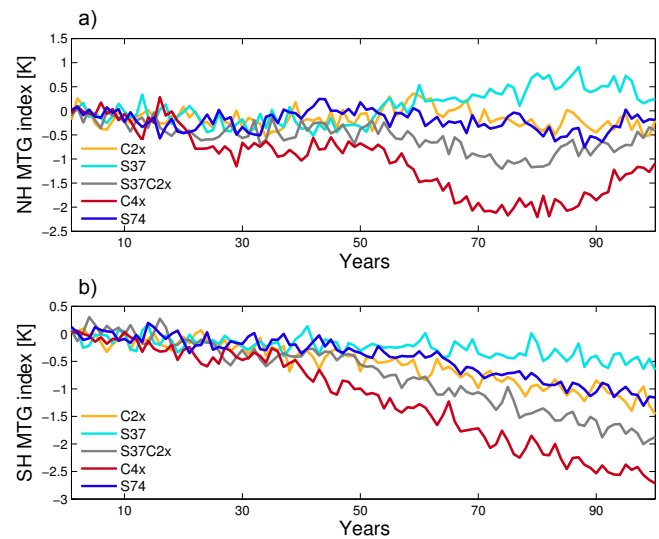
The different changes in convective precipitation, between CO_2 and solar scenarios, seem to follow the changes in surface temperature shown in Fig. 1b–d. Convective precipitation increases more in the tropics and mid-latitudes in solar scenarios due to the stronger warming, while in the high latitudes the convective precipitation response is larger in CO_2 scenarios due to the stronger polar amplification (see Figs. 5c and 1d). According to Held and Soden (2006), the decrease in convective mass flux should be smaller in solar simulations due to a smaller difference between the increase in moisture and precipitation. This would be in line with the stronger increase in convective precipitation in solar compared to CO_2 scenarios in the tropics, while the changes in the other sub-regions are more comparable (see Fig. 5a–c). However, in the CCSM3.5 model, the stronger hydrological sensitivity to solar forcing compared to CO_2 forcing per unit of surface warming is primarily caused by a larger increase in large-scale precipitation (see Fig. 3b). Figure 5d–f further shows that the main difference between CO_2 and solar scenarios arises in the mid-latitudes, where large-scale precipitation decreases in CO_2 scenarios but increases slightly in solar scenarios.

The responses in large-scale precipitation are complex to interpret, as they not only depend on energetic and thermodynamic constraints but also on changes in atmospheric circulation in the system. Therefore, changes in the pole-to-equator surface air temperature gradient are calculated to investigate changes in atmospheric circulation. We use an adapted version of the meridional temperature gradient (MTG) index defined by Gitelman et al. (1997) to quantify differences between the scenarios. Using the sub-regions defined above,
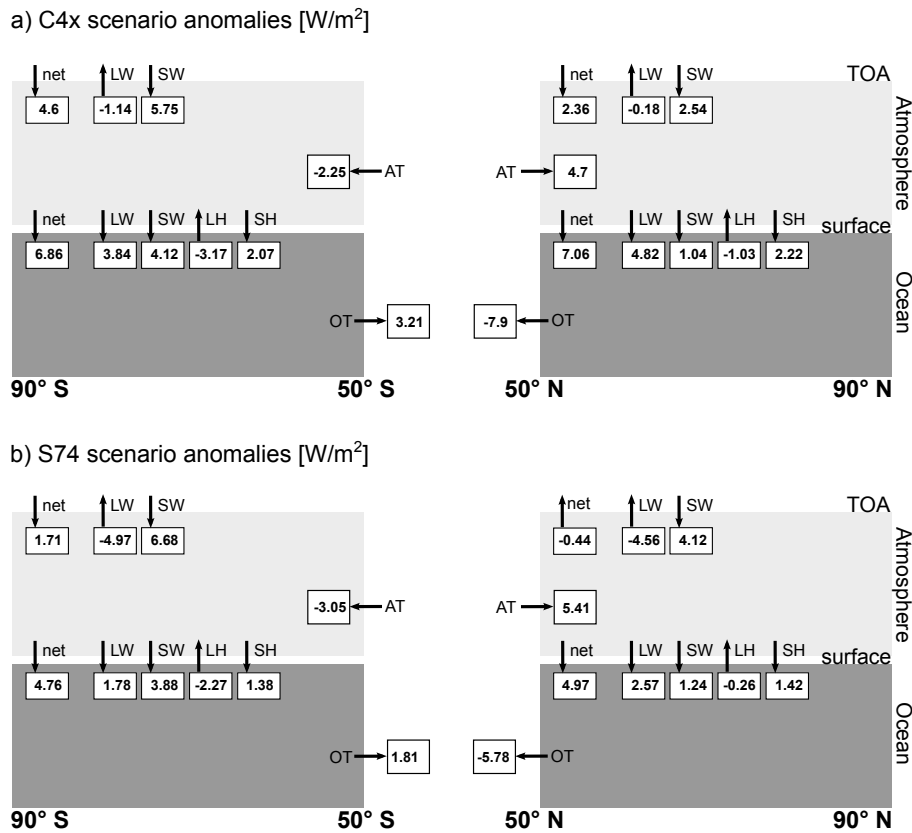
Fig. 7. Annual mean anomalies of the Earth's energy budget components for **(a)** the C4x and **(b)** the S74 simulation. The energy budget anomalies are calculated for two boxes (90° S to 50° S and 50° N to 90° N) and the change in poleward atmospheric energy transport (AT) is also indicated. Values are in W m^{-2} and energy fluxes are defined as positive downward and northward.

we calculate an MTG index in each hemisphere as the difference between the respective high latitudes and the tropics. With increasing global mean temperature and as already observed, Gitelman et al. (1997) showed that the MTG decreases, leading to weaker mid-latitudes eddies. In our simulations, the pole-to-equator gradient in the Southern Hemisphere decreases for all scenarios, in particular in the CO$_2$ cases (see Fig. 6b). In the Northern Hemisphere, the MTG index also decreases except for S37 where it slightly increases, which, according to Gitelman et al. (1997), would imply stronger mid-latitudes eddies (see Fig. 6a). The fact that the NH MTG index is not changing much for C2x, S74 and S37C2x is due to a cold anomaly in the North Atlantic caused by the weakening of the AMOC. The average temperature change in the northern high latitudes is therefore similar to the change in surface temperature in the tropics because the strong warming caused by polar amplification is damped by the cold anomaly in the North Atlantic.

Finally, energy budgets for the C4x and S74 simulations are calculated in both high latitude boxes (90° S to 50° S and 50° N to 90° N) to quantify the changes in poleward energy transport through the atmosphere. The poleward atmospheric heat transport (AT) is calculated as the difference between the net energy flux at top of atmosphere and the net energy flux at surface in each box. In the last 30 yr of constant forcing the atmosphere is in quasi-equilibrium and thus we assume zero heat storage in the high latitude boxes to calculate the meridional atmospheric energy transport (AT) as in Rugenstein et al. (2013). Figure 7 shows that the net TOA energy flux anomaly is much larger in C4x for both boxes and interestingly, it is even negative in the northern high latitudes in S74. While the net surface energy flux anomalies are more similar between CO$_2$ and solar simulation, the separation in LW, LH and SH appears more forcing-dependent. Note that the anomalies shown are not scaled, but scaling them with the adjusted forcing would make the anomalies in S74 increase, or decrease if negative, relative to the anomalies in C4x. As a consequence of the difference between both scenarios in the net TOA energy flux anomalies, the increase in poleward energy transport through the atmosphere is significantly larger in solar scenarios (AT in Fig. 7). Since a solar forcing increase acts primarily in the tropics, the energy received has to be redistributed. In contrast, a CO$_2$ forcing is homogeneously distributed over the globe and produces a stronger polar amplification, causing the temperature difference between poles and equator to decrease. Therefore, the

climate system maintains a stronger atmospheric circulation in solar compared to CO_2 scenarios, but in both scenarios the atmospheric circulation is weaker compared to the control simulation. Given that moisture increases in both scenarios compared to the control simulation, the same or a larger transport of energy, as Fig. 7 shows, can still be achieved by a weaker atmospheric circulation (Trenberth, 2011). Although large-scale precipitation depends not only on the poleward atmospheric energy transport, the presented results are well in line with the fact that large-scale precipitation increases more in solar scenarios compared to CO_2 scenarios at higher latitudes (see Fig. 5e, f).

4   Conclusions

In order to better understand changes in the energy budget and hydrological cycle in a warmer climate, idealized simulations are performed with the NCAR CCSM3.5 model. The scenarios are also designed to test the assumption of linear additivity of the response to different forcing agents and magnitudes in a fully coupled climate model for transient climate change. The responses of most variables of the energy budget and hydrological cycle do not add linearly in the 30 yr after stabilization in the global mean. The fact that most climate variables as simulated by CCSM3.5 do not respond linearly to forcings can be relevant for detection and attribution and pattern scaling techniques. Depending on the application, the errors introduced by assuming linear additivity when it does not apply might be considered negligible or not. In any case, these results cannot be captured properly by models of lower complexity, which are often used to inform policymakers or for impact studies, and are implicit when characterizing the overall magnitude of climate change or a target for stabilization in terms of global mean temperature or total radiative forcing. The linear additivity assumption is also tested for surface temperature, large-scale and convective precipitation in the tropics, mid-latitudes and high latitudes and appears to be not valid in general, regardless of the sub-region considered.

The best estimate of the radiative forcing of a doubling of CO_2 provided by Myhre et al. (1998) is often used in the literature to construct a solar simulation of the same intensity. This is what is done here but the temperature response to solar forcing is found to be significantly smaller than CO_2 forcing, as shown in previous studies (e.g. Hansen et al., 2005; Schmidt et al., 2012). On the one hand, this is due to the fact that the efficacy of solar forcing is smaller than the efficacy of CO_2 forcing, but on the other hand, the adjusted forcing of a quadrupling of CO_2 appeared to be more than twice the best estimate for a CO_2 doubling provided by Myhre et al. (1998) due to a reduced Planck response for higher LW emission levels (Good et al., 2012). This outcome indicates limitations in the traditional definition of radiative forcing. It is therefore central to consider the efficacy of a forcing agent (Hansen

et al., 2005), but also alternative techniques for calculating forcings (e.g. Hansen et al., 2002; Shine et al., 2003).

Following Andrews (2009), the forcing and feedback-dependent terms are calculated and the non-linear response in precipitation is shown to be caused by the feedback-dependent term. To provide new insights on reasons for the weaker increase in precipitation in CO_2 compared to solar forcing scenarios, the physical processes altering the components of the energy budget and hydrological cycle in the CCSM3.5 model are analyzed. When the raw modelled responses are considered and no scaling performed, surface warming appears weaker in solar compared to CO_2 scenarios. Given the Clausius–Clapeyron relationship, the water vapor increase in the lower troposphere follows the temperature increase and is therefore also weaker in solar scenarios. At the same time, the energy available for evaporation, and consequently precipitation as both are equal in the global annual mean, is larger in the unscaled solar scenarios. For the unscaled CO_2 scenarios, the opposite is true: the water vapor increase is relatively strong but the precipitation increase is relatively weak compared to solar scenarios. A weaker circulation is necessitated when the precipitation response is more muted relative to the water vapor response. This is illustrated by the longer residence times in CO_2 scenarios compared to solar scenarios. Finally, these conclusions are supported by the fact that the decrease in meridional temperature gradient expected with global warming is larger in the CO_2 case, indicating that less energy is available for mid-latitude eddies. Energy budgets over high latitude boxes in each hemisphere confirm that the poleward energy transport in the atmosphere increases more in solar scenarios. These results are in line with the stronger increase in large-scale precipitation in solar scenarios, while the increase in convective precipitation is more similar between CO_2 and solar forcing scenarios. Scaling the responses in each scenario by their corresponding adjusted forcing as is done to test the linear additivity assumption leads to the same conclusions.

It is important to stress that the presented results are based on one global climate model and cannot claim universal validity. Still, it would be useful to compare them with the same scenarios performed with different GCMs to assess whether the described processes are robust. For the IPCC reports, the focus is on comparing the models running the SRES and RCP scenarios where the composition of the forcings is complex. Pendergrass and Hartmann (2012) showed that in simulations used for the IPCC Fourth Assessment Report (IPCC, 2007) the black carbon forcing was not specified and was therefore different in each model, making model inter-comparison with such simulations difficult to interpret. Understanding how individual models respond to a given forcing is only possible with idealized simulations as presented in this study. We suggest that this could represent a systematic way to inter-compare and to some extent evaluate the models, and might provide additional information to classical model evaluations against observed climatological mean fields.

The ability to reproduce the observed climate is a priority in model inter-comparisons, but since observational errors remain substantial, in particular over oceans for precipitation (Liu et al., 2012), inter-comparing models in simple and idealized simulations might represent a complementary tool. Simulations with a one percent per year increase in CO_2 are available in the CMIP archive and one could imagine that the modeling groups could perform similar experiments with solar forcing only, and even with aerosol forcing. Then robust physical responses across the models could be identified and used as a complementary piece of information.

Edited by: V. Lucarini

References

Alessandri, A., Fogli, P., Vichi, M., and Zeng, N.: Strengthening of the hydrological cycle in future scenarios: atmospheric energy and water balance perspective, Earth Syst. Dynam., 3, 199–212, doi:10.5194/esd-3-199-2012, 2012.

Allan, R. P.: Variability in clear-sky longwave radiative cooling of the atmosphere, J. Geophys. Res.-Atmos., 111, D22105, doi:10.1029/2006JD007304, 2006.

Allen, M. R. and Ingram, W. J.: Constraints on future changes in climate and the hydrologic cycle, Nature, 419, 224–232, doi:10.1038/nature01092, 2002.

Andrews, T.: Forcing and response in simulated 20th and 21st century surface energy and precipitation trends, J. Geophys. Res.-Atmos., 114, D17110, doi:10.1029/2009JD011749, 2009.

Andrews, T. and Forster, P. M.: CO_2 forcing induces semi-direct effects with consequences for climate feedback interpretations, Geophys. Res. Lett., 35, L04802, doi:10.1029/2007GL032273, 2008.

Andrews, T. and Forster, P. M.: The transient response of global-mean precipitation to increasing carbon dioxide levels, Environ. Res. Lett., 5, 025212, doi:10.1088/1748-9326/5/2/025212, 2010.

Andrews, T., Forster, P. M., and Gregory, J. M.: A Surface Energy Perspective on Climate Change, J. Climate, 22, 2557–2570, doi:10.1175/2008JCLI2759.1, 2009.

Andrews, T., Forster, P. M., Boucher, O., Bellouin, N., and Jones, A.: Precipitation, radiative forcing and global temperature change, Geophys. Res. Lett., 37, L14701, doi:10.1029/2010GL043991, 2010.

Andrews, T., Doutriaux-Boucher, M., Boucher, O., and Forster, P. M.: A regional and global analysis of carbon dioxide physiological forcing and its impact on climate, Clim. Dynam., 36, 783–792, doi:10.1007/s00382-010-0742-1, 2011.

Andrews, T., Ringer, M. A., Doutriaux-Boucher, M., Webb, M. J., and Collins, W. J.: Sensitivity of an Earth system climate model to idealized radiative forcing, Geophys. Res. Lett., 39, L10702, doi:10.1029/2012GL051942, 2012.

Bala, G., Duffy, P. B., and Taylor, K. E.: Impact of geoengineering schemes on the global hydrological cycle, Proc. Natl. Acad. Sci. USA, 105, 7664–7669, doi:10.1073/pnas.0711648105, 2008.

Bala, G., Caldeira, K., and Nemani, R.: Fast versus slow response in climate change: implications for the global hydrological cycle, Clim. Dynam., 35, 423–434, doi:10.1007/s00382-009-0583-y, 2010.

Barnett, T., Zwiers, F., Hegerl, G., Allen, M., Crowley, T., Gillett, N., Hasselmann, K., Jones, P., Santer, B., Schnur, R., Scott, P., Taylor, K., and Tett, S.: Detecting and attributing external influences on the climate system: A review of recent advances, J. Climate, 18, 1291–1314, 2005.

Bender, F. A.-M.: Planetary albedo in strongly forced climate, as simulated by the CMIP3 models, Theor. Appl. Climatol., 105, 529–535, doi:10.1007/s00704-011-0411-2, 2011.

Boer, G. J.: Climate change and the regulation of the surface moisture and energy budgets, Clim. Dynam., 8, 225–239, 1993.

Bosilovich, M. G., Schubert, S. D., and Walker, G. K.: Global changes of the water cycle intensity, J. Climate, 18, 1591–1608, 2005.

Bosilovich, M. G., Chen, J. Y., Robertson, F. R., and Adler, R. F.: Evaluation of global precipitation in reanalyses, J. Appl. Meteorol. Climatol., 47, 2279–2299, doi:10.1175/2008JAMC1921.1, 2008.

Boville, B. A., Rasch, P. J., Hack, J. J., and McCaa, J. R.: Representation of clouds and precipitation processes in the Community Atmosphere Model version 3 (CAM3), J. Climate, 19, 2184–2198, doi:10.1175/JCLI3749.1, 2006.

Cao, L., Bala, G., and Caldeira, K.: Why is there a short-term increase in global precipitation in response to diminished CO_2 forcing?, Geophys. Res. Lett., 38, L046713, doi:10.1029/2011GL046713, 2011.

Cao, L., Bala, G., and Caldeira, K.: Climate response to changes in atmospheric carbon dioxide and solar irradiance on the time scale of days to weeks, Environ. Res. Lett., 7, 34015–34015, 2012.

Collins, W. D., Bitz, C. M., Blackmon, M. L., Bonan, G. B., Bretherton, C. S., Carton, J. A., Chang, P., Doney, S. C., Hack, J. J., Henderson, T. B., Kiehl, J. T., Large, W. G., McKenna, D. S., Santer, B. D., and Smith, R. D.: The Community Climate System Model version 3 (CCSM3), J. Climate, 19, 2122–2143, 2006.

Douville, H., Chauvin, F., Planton, S., Royer, J. F., Salas-Melia, D., and Tyteca, S.: Sensitivity of the hydrological cycle to increasing amounts of greenhouse gases and aerosols, Clim. Dynam., 20, 45–68, doi:10.1007/s00382-002-0259-3, 2002.

Forster, P. M., Andrews, T., Good, P., Gregory, J. M., Jackson, L. S., and Zelinka , M.: Evaluating adjusted forcing and model spread for historical and future scenarios in the CMIP5 generation of climate models, J. Geophys. Res.-Atmos., 118, 1139–1150, doi:10.1002/jgrd.50174, 2013.

Gent, P. R., Yeager, S. G., Neale, R. B., Levis, S., and Bailey, D. A.: Improvements in a half degree atmosphere/land version of the CCSM, Clim. Dynam., 34, 819–833, doi:10.1007/s00382-009-0614-8, 2010.

Gillett, N. P., Weaver, A. J., Zwiers, F. W., and Wehner, M. F.: Detection of volcanic influence on global precipitation, Geophys. Res. Lett., 31, L12217, doi:10.1029/2004GL020044, 2004.

Giorgi, F.: A simple equation for regional climate change and associated uncertainty, J. Climate, 21, 1589–1604, doi:10.1175/2007JCLI1763.1, 2008.

Gitelman, A. I., Risbey, J. S., Kass, R. E., and Rosen, R. D.: Trends in the surface meridional temperature gradient, Geophys. Res. Lett., 24, 1243–1246, 1997.

Good, P., Ingram, W., Lambert, F. H., Lowe, J. A., Gregory, J. M., Webb, M. J., Ringer, M. A., and Wu, P.: A step-response approach for predicting and understanding non-linear precipitation

changes, Clim. Dynam., 39, 2789–2803, doi:10.1007/s00382-012-1571-1, 2012.

Gregory, J. M. and Forster, P. M.: Transient climate response estimated from radiative forcing and observed temperature change, J. Geophys. Res.-Atmos., 113, D23105, doi:10.1029/2008JD010405, 2008.

Gregory, J. M. and Webb, M.: Tropospheric adjustment induces a cloud component in CO_2 forcing, J. Climate, 21, 58–71, doi:10.1175/2007JCLI1834.1, 2008.

Gregory, J. M., Ingram, W. J., Palmer, M. A., Jones, G. S., Stott, P. A., Thorpe, R. B., Lowe, J. A., Johns, T. C., and Williams, K. D.: A new method for diagnosing radiative forcing and climate sensitivity, Geophys. Res. Lett., 31, L018747, doi:10.1029/2003GL018747, 2004.

Hansen, J., Sato, M., Nazarenko, L., Ruedy, R., Lacis, A., Koch, D., Tegen, I., Hall, T., Shindell, D., Santer, B., Stone, P., Novakov, T., Thomason, L., Wang, R., Wang, Y., Jacob, D., Hollandsworth, S., Bishop, L., Logan, J., Thompson, A., Stolarski, R., Lean, J., Willson, R., Levitus, S., Antonov, J., Rayner, N., Parker, D., and Christy, J.: Climate forcings in Goddard Institute for Space Studies SI2000 simulations, J. Geophys. Res.-Atmos., 107, 4347, doi:10.1029/2001JD001143, 2002.

Hansen, J., Sato, M., Ruedy, R., Nazarenko, L., Lacis, A., Schmidt, G. A., Russell, G., Aleinov, I., Bauer, M., Bauer, S., Bell, N., Cairns, B., Canuto, V., Chandler, M., Cheng, Y., Del Genio, A., Faluvegi, G., Fleming, E., Friend, A., Hall, T., Jackman, C., Kelley, M., Kiang, N., Koch, D., Lean, J., Lerner, J., Lo, K., Menon, S., Miller, R., Minnis, P., Novakov, T., Oinas, V., Perlwitz, J., Perlwitz, J., Rind, D., Romanou, A., Shindell, D., Stone, P., Sun, S., Tausnev, N., Thresher, D., Wielicki, B., Wong, T., Yao, M., and Zhang, S.: Efficacy of climate forcings, J. Geophys. Res.-Atmos., 110, D18104, doi:10.1029/2005JD005776, 2005.

Held, I. M. and Soden, B. J.: Robust responses of the hydrological cycle to global warming, J. Climate, 19, 5686–5699, 2006.

IPCC: Climate change 2007: The physical science basis. Contribution of Working Group I to the Fourth Assessment Report of the Intergovernmental Panel on Climate Change, edited by: Solomon, S., Qin, D., Manning, M., Chen, Z., Marquis, M., Averyt, K. B., Tignor, M., and Miller, H. L., Cambridge University Press, Cambridge, United Kingdom and New York, NY, USA, p. 996, 2007.

Jonko, A. K., Shell, K. M., Sanderson, B. M., and Danabasoglu, G.: Climate Feedbacks in CCSM3 under Changing CO_2 Forcing. Part I: Adapting the Linear Radiative Kernel Technique to Feedback Calculations for a Broad Range of Forcings, J. Climate, 25, 5260–5272, doi:10.1175/JCLI-D-11-00524.1, 2012.

Kiehl, J. T. and Trenberth, K. E.: Earth's annual global mean energy budget, B. Am. Meteorol. Soc., 78, 197–208, 1997.

Knutti, R. and Stocker, T. F.: Influence of the thermohaline circulation on projected sea level rise, J. Climate, 13, 1997–2001, doi:10.1175/1520-0442(2000)013<1997:IOTTCO>2.0.CO;2, 2000.

Knutti, R., Allen, M. R., Friedlingstein, P., Gregory, J. M., Hegerl, G. C., Meehl, G. A., Meinshausen, M., Murphy, J. M., Plattner, G. K., Raper, S. C. B., Stocker, T. F., Stott, P. A., Teng, H., and Wigley, T. M. L.: A review of uncertainties in global temperature projections over the twenty-first century, J. Climate, 21, 2651–2663, doi:10.1175/2007JCLI2119.1, 2008.

Lambert, F. H. and Allen, M. R.: Are Changes in Global Precipitation Constrained by the Tropospheric Energy Budget?, J. Climate, 22, 499–517, doi:10.1175/2008JCLI2135.1, 2009.

Lambert, F. H. and Faull, N. E.: Tropospheric adjustment: The response of two general circulation models to a change in insolation, Geophys. Res. Lett., 34, L03701, doi:10.1029/2006GL028124, 2007.

Levitus, S., Antonov, J. I., Wang, J. L., Delworth, T. L., Dixon, K. W., and Broccoli, A. J.: Anthropogenic warming of Earth's climate system, Science, 292, 267–270, doi:10.1126/science.1058154, 2001.

Liepert, B. G. and Previdi, M.: Do Models and Observations Disagree on the Rainfall Response to Global Warming?, J. Climate, 22, 3156–3166, 2009.

Liu, C., Allan, R. P., and Huffman, G. J.: Co-variation of temperature and precipitation in CMIP5 models and satellite observations, Geophys. Res. Lett., 39, L13803, doi:10.1029/2012GL052093, 2012.

Meehl, G. A., Washington, W. M., Wigley, T. M. L., Arblaster, J. M., and Dai, A.: Solar and greenhouse gas forcing and climate response in the twentieth century, J. Climate, 16, 426–444, 2003.

Meehl, G. A., Washington, W. M., Ammann, C. M., Arblaster, J. M., Wigley, T. M. L., and Tebaldi, C.: Combinations of natural and anthropogenic forcings in twentieth-century climate, J. Climate, 17, 3721–3727, 2004.

Meehl, G. A., Stocker, T. F., Collins, W. D., Friedlingstein, P., Gaye, A. T., Gregory, J. M., Kitoh, A., Knutti, R., Murphy, J. M., Noda, A., Raper, S. C. B., Watterson, I. G., Weaver, A. J., and Zhao, Z.-C.: Global climate projections, Climate Change 2007: The Physical Science Basis. Contribution of Working Group I to the Fourth Assessment Report of the Intergovernmental Panel on Climate Change, edited by: Solomon, S., Qin, D., Manning, M., Chen, Z., Marquis, M., Averyt, K. B., Tignor, M. and Miller, H. L., Cambridge University Press, Cambridge, United Kingdom and New York, NY, USA, 2007.

Mitchell, J. F. B., Wilson, C. A., and Cunnington, W. M.: On CO_2 climate sensitivity and model dependence of results, Q. J. Roy. Meteorol. Soc., 113, 293–322, 1987.

Mitchell, T. D.: Pattern scaling – An examination of the accuracy of the technique for describing future climates, Clim. Change, 60, 217–242, 2003.

Mitchell, T. D. and Hulme, M.: Predicting regional climate change: living with uncertainty, Prog. Phys. Geogr., 23, 57–78, doi:10.1191/030913399672023346, 1999.

Moss, R. H., Edmonds, J. A., Hibbard, K. A., Manning, M. R., Rose, S. K., van Vuuren, D. P., Carter, T. R., Emori, S., Kainuma, M., Kram, T., Meehl, G. A., Mitchell, J. F. B., Nakicenovic, N., Riahi, K., Smith, S. J., Stouffer, R. J., Thomson, A. M., Weyant, J. P., and Wilbanks, T. J.: The next generation of scenarios for climate change research and assessment, Nature, 463, 747–756, doi:10.1038/nature08823, 2010.

Myhre, G., Highwood, E. J., Shine, K. P., and Stordal, F.: New estimates of radiative forcing due to well mixed greenhouse gases, Geophys. Res. Lett., 25, 2715–2718, 1998.

O'Gorman, P. A., Allan, R. P., Byrne, M. P., and Previdi, M.: Energetic Constraints on Precipitation Under Climate Change, Surv. Geophys., 33, 585–608, doi:10.1007/s10712-011-9159-6, 2012.

Pendergrass, A. G. and Hartmann, D. L.: Global-mean precipitation and black carbon in AR4 simulations, Geophys. Res. Lett., 39, L01703, doi:10.1029/2011GL050067, 2012.

Rugenstein, M. A. A., Winton, M., Stouffer, R. J., Griffies, S. M., and Hallberg, R.: Northern high latitude heat budget decomposition and transient warming, J. Climate, 26, 609–621, doi:10.1175/JCLI-D-11-00695.1, 2013.

Ruosteenoja, K., Tuomenvirta, H., and Jylha, K.: GCM-based regional temperature and precipitation change estimates for Europe under four SRES scenarios applying a super-ensemble pattern-scaling method, Clim. Change, 81, 193–208, doi:10.1007/s10584-006-9222-3, 2007.

Santer, B. D. and Wigley, T. M. L.: Regional validation of means, variances, and spatial patterns in general-circulation model control runs, J. Geophys. Res.-Atmos., 95, 829–850, doi:10.1029/JD095iD01p00829, 1990.

Schaller, N., Mahlstein, I., Cermak, J., and Knutti, R.: Analyzing precipitation projections: A comparison of different approaches to climate model evaluation, J. Geophys. Res.-Atmos., 116, D014963, doi:10.1029/2010JD014963, 2011.

Schmidt, H., Alterskjær, K., Bou Karam, D., Boucher, O., Jones, A., Kristjánsson, J. E., Niemeier, U., Schulz, M., Aaheim, A., Benduhn, F., Lawrence, M., and Timmreck, C.: Solar irradiance reduction to counteract radiative forcing from a quadrupling of CO_2: climate responses simulated by four earth system models, Earth Syst. Dynam., 3, 63–78, doi:10.5194/esd-3-63-2012, 2012.

Shine, K. P., Cook, J., Highwood, E. J., and Joshi, M. M.: An alternative to radiative forcing for estimating the relative importance of climate change mechanisms, Geophys. Res. Lett., 30, 2047, doi:10.1029/2003GL018141, 2003.

Shiogama, H., Emori, S., Takahashi, K., Nagashima, T., Ogura, T., Nozawa, T., and Takemura, T.: Emission scenario dependency of precipitation on global warming in the MIROC3.2 model, J. Climate, 23, 2404–2417, 2010a.

Shiogama, H., Hanasaki, N., Masutomi, Y., Nagashima, T., Ogura, T., Takahashi, K., Hijioka, Y., Takemura, T., Nozawa, T., and Emori, S.: Emission scenario dependencies in climate change assessments of the hydrological cycle, Clim. Change, 99, 321–329, 2010b.

Stephens, G. L.: Cloud feedbacks in the climate system: A critical review, J. Climate, 18, 237–273, 2005.

Stephens, G. L. and Ellis, T. D.: Controls of Global-Mean Precipitation Increases in Global Warming GCM Experiments, J. Climate, 21, 6141–6155, doi:10.1175/2008JCLI2144.1, 2008.

Stouffer, R. J.: Time scales of climate response, J. Climate, 17, 209–217, doi:10.1175/1520-0442(2004)017<0209:TSOCR>2.0.CO;2, 2004.

Sutton, R. T., Dong, B., and Gregory, J. M.: Land/sea warming ratio in response to climate change: IPCC AR4 model results and comparison with observations, Geophys. Res. Lett., 34, L02701, doi:10.1029/2006GL028164, 2007.

Trenberth, K. E.: Changes in precipitation with climate change, Clim. Res., 47, 123–138, doi:10.3354/cr00953, 2011.

Trenberth, K. E., Fasullo, J. T., and Kiehl, J.: Earth'S Global Energy Budget, B. Am. Meteorol. Soc., 90, 311–323, doi:10.1175/2008BAMS2634.1, 2009.

Watterson, I. G.: Calculation of probability density functions for temperature and precipitation change under global warming, J. Geophys. Res.-Atmos., 113, D12106, doi:10.1029/2007JD009254, 2008.

Wild, M., Grieser, J., and Schaer, C.: Combined surface solar brightening and increasing greenhouse effect support recent intensification of the global land-based hydrological cycle, Geophys. Res. Lett., 35, L17706, doi:10.1029/2008GL034842, 2008.

Zelinka, M. D. and Hartmann, D. L.: Why is longwave cloud feedback positive?, J. Geophys. Res.-Atmos., 115, D16117, doi:10.1029/2010JD013817, 2010.

Zhang, M. H., Lin, W. Y., Klein, S. A., Bacmeister, J. T., Bony, S., Cederwall, R. T., Del Genio, A. D., Hack, J. J., Loeb, N. G., Lohmann, U., Minnis, P., Musat, I., Pincus, R., Stier, P., Suarez, M. J., Webb, M. J., Wu, J. B., Xie, S. C., Yao, M. S., and Zhang, J. H.: Comparing clouds and their seasonal variations in 10 atmospheric general circulation models with satellite measurements, J. Geophys. Res.-Atmos., 110, D005021, doi:10.1029/2004JD005021, 2005.